Performance Comparison of LDPC Codes using SRK Equalisation and OFDM Techniques for Broadband Fixed Wireless Access Systems

M K Khan[1], R.A. Carrasco[1], I.J.Wassell[2], J.A.Neasham[1]

1. Communications and Signal Processing Group, School of EE&C Engineering,

University of Newcastle-upon-Tyne

E-mail: {m.k.khan, r.carrasco, j.a.neasham}@ newcastle.ac.uk

2. Digital Technology Group, Computer Laboratory,

University of Cambridge

E-mail: ijw24@cam.ac.uk

Abstract - Broadband Fixed Wireless Access (BFWA) systems enable services such as high-speed data communication, high quality voice/video conferencing and high-speed Internet access in areas where a wired link is not possible. However, the BFWA channel is a slow fading channel having deep frequency selective fading caused by clusters of scatterers in the environment that introduce inter-symbol interference (ISI) at the receiver. In this paper, Low Density Parity Check (LDPC) codes, optimised for the SISO BFWA channel, are designed using the structured Balance Incomplete Block Design (BIBD) method. The use of both QPSK and 16-QAM modulation are investigated theoretically. To help overcome the ISI effects of the channel, equalisation techniques are employed separately with LDPC decoding for a system employing QPSK and 16-QAM modulation schemes. The equaliser single carrier approach is then replaced with orthogonal frequency division multiplexing (OFDM) and the performance of these two approaches is evaluated in terms of bit-error rate. The simulation results show that equalisation with LDPC coding has a measurable performance gain over LDPC coding with OFDM.

Index Terms **-** LDPC codes, BFWA channel, Equalisation, BIBD Design, OFDM, WiMAX or IEEE 802.16

This work has been funded by the EPSRC, Grant No. GS/ S46444 /02**.**

1. Introduction

Broadband fixed wireless access (BFWA) [1] systems offer a solution to the problem of providing inexpensive broadband services from the local exchange to the customer. It can be deployed quickly, covering a large area with low cost compared to cable installations. A BFWA system can provide traditional voice, data, voice over internet protocol VOIP, remote education, video conference, high-speed internet access etc. Achieving high data rates in wireless communication environments is limited by multipath fading between transmitter and receiver degrading the system performance. The transmitted data through the broadband fixed wireless channel is subject to attenuation and distortion by various factors such as foliage, buildings, precipitation, and vehicles etc. Therefore, there is a need to use a model which is parameterised according to the various terrain and environments experienced by BFWA systems. The Stanford University Interim (SUI) channel model [2] has been developed specifically for fixed wireless systems and takes into account a number of parameters for example, Doppler effect, path loss, multipath delay spread and fading characteristics. Consequently it has been chosen to model the BFWA channel in this paper.

The IEEE working group on Broadband Wireless Access Standards are developing IEEE 802.16 [3], which provides the standards for broadband wireless system implementation. As part of the specification the use of OFDM has been proposed in order to combat frequency selective fading in the BFWA channel. Also, the use of space diversity for capacity improvement using OFDM has been analysed in [4]. This paper also discusses the physical layer research challenges in MIMO-OFDM BFWA systems, including physical channel measurements and modelling, analogue beam forming techniques using adaptive antenna arrays, space-time techniques for MIMO-OFDM, error control coding techniques etc. In [5], a broadband multiple-input multiple-output (MIMO) OFDM system has been designed and evaluated for a fixed wireless link between tall buildings in an urban area.

Moreover, there has been a lot of emphasis on joint equalisation and decoding of coded systems. The application of the turbo principle [6] to iterative decoding and demodulation has provided significant gains [7]. Such systems are essentially serial concatenation schemes [8] with the ISI channel as the inner code. The aim of the research described in this paper is to design and analyse the performance of two single input single output (SISO) BFWA systems. The first system uses a single carrier approach with a Square Root Kalman (SRK) equaliser in conjunction with some newly generated LDPC codes using Balanced Incomplete Block Design (BIBD) [9]. For a BFWA system, it is important to design LDPC codes with very high code rates to minimise the redundant information that is introduced and hence maintain a high data rate. At the same time, the code must also have a very good error-correcting capability which implies that it must have a large code length. The BIBD construction method produces LDPC codes with large lengths and high code rates greater than 0.9 that outperform randomly constructed LDPC codes with similar parameters. A second advantage of using this scheme is its reduced encoding complexity, which is important in reducing the overall delay of the BFWA system.

The second scheme replaces the single carrier approach with one employing OFDM i.e., a SISO OFDM BFWA system. The scheme can easily be extended to MIMO BFWA systems.

The main aim of this paper to analyse the performance of high rate, low complexity LDPC codes with varying lengths with interference reduction techniques, such as equalization and OFDM, to improve the performance of the system. The high rate LDPC codes have been constructed by the authors using the BIBD construction method: the (2715, 2535) LDPC code of rate 0.934 and the (4351, 4123) LDPC code of rate 0.948. The theoretical analysis of the SISO BFWA system using non-coherent [16] detection for QPSK/ 16-QAM is also presented with simulation results. For coherent detection readers can refer to [21] which present the theoretical analysis of SISO/MIMO BFWA systems.

This paper is organised as follows: Section 2 presents the overall description of the fixed WiMAX (IEEE 802.16d) or BFWA system. The theoretical analysis of the BFWA channel by employing non-

coherent detection using QPSK and 16-QAM is presented in section 3. In Section 4, we briefly discuss the construction method, known as BIBD, of LDPC codes used for simulation in this paper. Then, an overview of the SRK equalisation technique is described in Section 5 along with the description of the sum-product decoding algorithm of LDPC codes. Section 6 compares the simulation results for the equalised system and un-equalised system. It also discusses the performance comparison of various LDPC codes using QPSK and QAM modulation schemes. Finally, section 7 summarises the main contributions of this paper.

2. System Model

The overall general system diagrams are shown in Figure 1. In Figure 1 (a), single carrier transmission with SRK equalisation has been used and in Figure 1 (b), OFDM has been used with the aim of overcoming the ISI introduced by the BFWA channel. In the transmitter the data bits b_k, generated by the source, are encoded by the LDPC encoder into encoded bits c_n. The block interleaver re-orders the encoded bits and the modulator maps them into QPSK or QAM symbols s_n. In Figure 1(a) this signal (represented by x_n) is modulated onto a single carrier for use in the equalised system, whereas in Figure 1(b) the signal is fed into an OFDM modulator. In the initial stage of OFDM modulation, the symbol stream from the mapper is converted from serial to parallel and then an Inverse Fast Fourier Transform IFFT is applied. Finally a cyclic prefix (CP) is added to the signal x_n before transmitting over the SUI-3 multipath channel with three resolvable paths with tap spacings of 500ns and a total delay of 1000ns. The model can be considered as a 3-tap transversal filter with a finite impulse response. The Doppler Effect specified in our channel specification is also taken into account when calculating the taps coefficient values. The transmitted signal is also corrupted by additive white Gaussian noise (AWGN). The total power of all paths of the channel is normalized to unity, so that there is no gain provided by the dispersive channel. The channel filter coefficients are calculated and the transmitted sequence from the antennae is multiplied by these coefficients.

There are a number of SUI channel models specified in [2] depending upon the different terrain conditions. All of them have three resolvable paths with either Rician or Rayleigh amplitude distributions. The amplitude distribution of the SUI-3 channel model is Rician for the first path and Rayleigh for the other two paths.

Hence the received signal r_n can be expressed as

$$r_n = \alpha_0 x_n + \alpha_1 x_{n-1} + \alpha_2 x_{n-2} + z_n \quad \textbf{(1)}$$

where z_n is the complex additive white Gaussian noise (AWGN) and $\alpha_n \; \forall \;\; n = 0,1,2$ are the complex value coefficients.

The receiver aims to recover the original information bits from the received samples corrupted by the channel. For the equalised system, the received samples, r_n, are passed directly to the SRK equaliser to attempt to reduce ISI. After equalisation/demodulation of the received samples, the log-likelihood (LLR) values, $\hat{d}_n$, of each bit are calculated and passed to the block de-interleaver. The decoder applies the message passing algorithm on the de-interleaved bits, $\hat{c}_n$, in an iterative manner to extract estimates of the original information bits, $\hat{b}_k$.

For the OFDM system the received samples r_n are passed directly to the OFDM demodulator. After OFDM demodulation the received symbols are passed to the soft demapper where the LLR values of the received symbol are calculated before being passed to the de-interleaver and LDPC decoder.

3. Theoretical Analysis of BFWA Channel

In [16], Xiao *et al* presented the theoretical analysis of a BFWA system using coherent and non-coherent detection methods for both QPSK and QAM modulation scheme. The theoretical approach is necessary to analyze the effect of ISI on the performance of the BFWA systems, with an attempt to gain a deep insight into the physical limitations of the BFWA channels with conventional detection

techniques. There are six different channels for different terrain types defined in SUI-3 channel specification and we have chosen SUI-3 channel with three taps having tap delay of 500 ns between the adjacent taps. The analysis assumes that the length of one QPSK/QAM symbol is equal to the spacing between the adjacent taps which gives the data rate of 4Mbps with QPSK modulation and 8Mbps with 16-QAM. The channel coefficient is assumed to be constant during the transmission of one block of data; however, they vary from block to block. The transmitted QPSK/QAM symbol at time instant *n* is denoted as $x_n = x_n^I + jx_n^Q$, and z_n is the complex additive white Gaussian noise with zero mean and variance N_0.

The results in [16] shows there is a closed match between the simulated and theoretical results. For both QPSK and 16-QAM modulation the non-coherent detection is performed on the original received signal without correcting the phase shift. The simulation results of only non-coherent detection are presented and the authors have also mentioned the analysis of coherent detection for QPSK/ 16-QAM in [16] and [21]. The next sub-section briefly describes the theoretical approach for non-coherent detection of an M-PSK signal over the BFWA channel.

3.1 Performance of Non-coherent Detection on the BFWA Channel

The original signal r_n received from the channel is directly passed to the QPSK demodulator without correcting the phase shift. The received signal from the channel is given by Eq. (1) as

$$r_n = \alpha_o x_n + \underbrace{\alpha_1 x_{n-1} + \alpha_2 x_{n-2} + z_n}_{\text{Combined ISI and Noise}} = \alpha_0 x_n + w_n \qquad \textbf{(2)}$$

where $w_n = \alpha_1 x_{n-1} + \alpha_2 x_{n-2} + z_n \sim \mathcal{N}(0, N_w)$ is combined ISI and Gaussian noise and it is assumed that w_n has a complex Gaussian distribution for a large number of channel instantiations. $N_w = \mathrm{E}\left[|\alpha_1|^2\right] + \mathrm{E}\left[|\alpha_2|^2\right] + N_0 = P_1 + P_2 + N_0$, where P_1 and P_2 are the powers of the second and third taps respectively and N_0 is noise power.

3.1.1 Non-coherent Detection for QPSK Modulation

The probability of a symbol error occurring, e.g. $\hat{x}_n = x_1$ given x_0 is transmitted can be computed as [16]

$$P(\hat{x}_n = x_1 \mid x_n = x_0) = P(\alpha_0 x_0 + w_n \in R_1) \tag{3}$$

where R_1 is the decision region for symbol x_1 in QPSK constellation, substituting $\alpha_0 = \alpha_I + j\alpha_Q$ and $x_0 = 1/\sqrt{2} + j\,1/\sqrt{2}$ in equation (3),

$$\begin{aligned}
&= P\left\{(\alpha_I + j\alpha_Q)\left(\frac{1}{\sqrt{2}} + j\frac{1}{\sqrt{2}}\right) + w_n \in R_1\right\} \\
&= P\left\{\frac{\alpha_I - \alpha_Q}{\sqrt{2}} + w_I < 0\right\} \cdot P\left\{\frac{\alpha_I + \alpha_Q}{\sqrt{2}} + w_Q > 0\right\} \\
&= Q\left(\frac{\alpha_I - \alpha_Q}{\sqrt{(P_1 + P_2 + N_0)}}\right) Q\left(-\frac{\alpha_I + \alpha_Q}{\sqrt{(P_1 + P_2 + N_0)}}\right)
\end{aligned} \tag{4}$$

Similarly, other conditional probabilities can be obtained as

$$P(\hat{x}_n = x_2 \mid x_n = x_0) = Q\left(\frac{\alpha_I - \alpha_Q}{\sqrt{(P_1 + P_2 + N_0)}}\right) Q\left(\frac{\alpha_I + \alpha_Q}{\sqrt{(P_1 + P_2 + N_0)}}\right) \tag{5}$$

$$P(\hat{x}_n = x_3 \mid x_n = x_0) = Q\left(-\frac{\alpha_I - \alpha_Q}{\sqrt{(P_1 + P_2 + N_0)}}\right) Q\left(\frac{\alpha_I + \alpha_Q}{\sqrt{(P_1 + P_2 + N_0)}}\right) \tag{6}$$

Let $X = \alpha_I - \alpha_Q$ and $Y = \alpha_I + \alpha_Q$ where the probability density function PDF of X and Y is given as

$$p(X) = \frac{1}{\sqrt{2\pi}\sigma} \exp\left[-\frac{(X)^2}{2\sigma^2}\right], \qquad -\infty \le X \le \infty \tag{7}$$

$$p(Y) = \frac{1}{\sqrt{2\pi}\sigma} \exp\left[-\frac{(Y - m_Y)^2}{2\sigma^2}\right], \qquad -\infty \le Y \le \infty \tag{8}$$

The signal constellation of QPSK is shown in Figure 2 (a) and the error event $(\hat{x}_n = x_2 \mid x_n = x_0)$ results in 2 bit errors while $(\hat{x}_n = x_1 \mid x_n = x_0)$ and $(\hat{x}_n = x_2 \mid x_n = x_0)$ result in 1 bit error. The bit error probability is therefore given as

$$P_b = \frac{1}{k}\left[2 \times P(\hat{x}_n = x_2 \mid x_n = x_0) + 1 \times P(\hat{x}_n = x_1 \mid x_n = x_0) + 1 \times P(\hat{x}_n = x_3 \mid x_n = x_0)\right] \tag{9}$$

where k is the number of bits per symbol for QPSK ($k = 2$). Therefore, Eq. (9) becomes

$$P_b(X,Y) = \frac{1}{2}\left[2\times Q\left(\frac{X}{\sqrt{N_w}}\right)Q\left(\frac{Y}{\sqrt{N_w}}\right) + Q\left(\frac{X}{\sqrt{N_w}}\right)Q\left(-\frac{Y}{\sqrt{N_w}}\right) + Q\left(-\frac{X}{\sqrt{N_w}}\right)Q\left(\frac{Y}{\sqrt{N_w}}\right)\right]$$

$$P_b(X,Y) = Q\left(\frac{X}{\sqrt{N_w}}\right)Q\left(\frac{Y}{\sqrt{N_w}}\right) + \frac{1}{2}Q\left(\frac{X}{\sqrt{N_w}}\right)Q\left(-\frac{Y}{\sqrt{N_w}}\right) + \frac{1}{2}Q\left(-\frac{X}{\sqrt{N_w}}\right)Q\left(\frac{Y}{\sqrt{N_w}}\right) \quad \textbf{(10)}$$

The average bit error probability $\overline{P}_b$ is derived by taking the expectation of $P_b(X,Y)$ expressed in Eq. (9) with respect to X and Y. Since X is a zero mean normal random variable then $\mathrm{E}[Q(\lambda X)] = Q(0) = 0.5$. Therefore expectation of Eq. (10) with respect to x is equivalent to Eq. (11) below and the proof is given in Appendix A

$$P_b(Y) = \frac{1}{4}Q\left(-\frac{Y}{\sqrt{N_w}}\right) + \frac{3}{4}Q\left(\frac{Y}{\sqrt{N_w}}\right) \quad \textbf{(11)}$$

If z is a zero-mean, unit-variance, normal random variable, then according to [28]

$$\mathrm{E}[Q(\mu + \lambda z)] = Q\left(\frac{\mu}{\sqrt{1+\lambda^2}}\right) \quad \textbf{(12)}$$

Assign $Z = (Y - m_Y)/\sigma$ such that Z is a zero-mean, unit-variance, normal random variable. By taking the expectation of Eq. (10), we derive the average bit error probability as

$$\overline{P}_b = E\left[\frac{1}{4}Q\left(-\frac{\sigma Z + m_Y}{\sqrt{N_w}}\right) + \frac{3}{4}Q\left(\frac{\sigma Z + m_Y}{\sqrt{N_w}}\right)\right]$$

$$\overline{P}_b = \frac{1}{4}Q\left(\frac{\mu_1}{\sqrt{1+\lambda_1^2}}\right) + \frac{3}{4}Q\left(\frac{\mu_2}{\sqrt{1+\lambda_2^2}}\right) \quad \textbf{(13)}$$

where $\lambda_1 = -\frac{\sigma}{\sqrt{N_w}}$, $\mu_1 = -\frac{m_Y}{\sqrt{N_w}}$, $\lambda_2 = \frac{\sigma}{\sqrt{N_w}}$, $\mu_2 = \frac{m_Y}{\sqrt{N_w}}$

3.1.2 Non-coherent Detection for 16-QAM

The constellation of 16-QAM showing different types of decision regions is shown in Figure 2 (b). Let us consider x_n is a type *a* symbol then the received signal r_n can be written as

$$
\begin{aligned}
r_n &= \alpha_0 x_n + w_n = (\alpha_I + j\alpha_Q)(A + jA) + w_n \\
&= A(\alpha_I - \alpha_Q) + w_I + jA(\alpha_I + \alpha_Q) + jw_Q
\end{aligned}
\tag{14}
$$

In this case, the probability of 1 error event along the *I* axis is different from 1 error event along the *Q* axis. They are denoted by P_{1I}, P_{1Q}, respectively. The probability of a 2-error event is denoted as P_2. These probabilities are computed as

$$
\begin{aligned}
P_{1I} &= P_r\{A(\alpha_I - \alpha_Q) + w_I < 0\} = P_r\{w_I < -A(\alpha_I - \alpha_Q)\} \\
&= P_r\left\{\frac{w_I}{\sqrt{N_w/2}} < -\frac{\sqrt{2}A(\alpha_I - \alpha_Q)}{\sqrt{N_w}}\right\} \\
&= Q\left[\frac{\sqrt{2}A(\alpha_I - \alpha_Q)}{\sqrt{N_w}}\right]
\end{aligned}
\tag{15}
$$

$$
\begin{aligned}
P_{1Q} &= P_r\{A(\alpha_I + \alpha_Q) + w_Q < 0\} = P_r\{w_Q < -A(\alpha_I + \alpha_Q)\} \\
&= P_r\left\{\frac{w_Q}{\sqrt{N_w/2}} < -\frac{\sqrt{2}A(\alpha_I + \alpha_Q)}{\sqrt{N_w}}\right\} \\
&= Q\left[\frac{\sqrt{2}A(\alpha_I + \alpha_Q)}{\sqrt{N_w}}\right]
\end{aligned}
\tag{16}
$$

$$
\begin{aligned}
P_2 &= P_r\{A(\alpha_I - \alpha_Q) + w_I < 0\} \cdot P_r\{A(\alpha_I + \alpha_Q) + w_Q < 0\} \\
&= Q\left[\frac{\sqrt{2}A(\alpha_I - \alpha_Q)}{\sqrt{N_w}}\right] Q\left[\frac{\sqrt{2}A(\alpha_I + \alpha_Q)}{\sqrt{N_w}}\right]
\end{aligned}
\tag{17}
$$

The conditional bit error probabilities P_a, P_b, P_c of decision region type *a*, b and *c* respectively is given as

$$
P_a = \frac{1}{4}\left[n_{a1I} \cdot P_{1I} + n_{a1Q} P_{1Q} + n_{a2} \cdot 2 \cdot P_2\right]
$$

$$= \frac{1}{4}\left[2P_{1I} + 2P_{1Q} + 8P_2\right] \quad \textbf{(18)}$$

$$P_b = \frac{1}{4}\left[n_{b1I} \cdot P_{1I} + n_{b1Q} P_{1Q} + n_{b2} \cdot 2 \cdot P_2\right]$$

$$= \frac{1}{4}\left[P_{1I} + 2P_{1Q} + 4P_2\right] \quad \textbf{(19)}$$

$$P_c = \frac{1}{4}\left[n_{c1I} \cdot P_{1I} + n_{c1Q} P_{1Q} + n_{c2} \cdot 2 \cdot P_2\right]$$

$$= \frac{1}{4}\left[P_{1I} + P_{1Q} + 2P_2\right] \quad \textbf{(20)}$$

where n_{a1I}, n_{a1Q} represents the number of regions that differ by 1 bit from transmitted type *a* and along the I/Q axis, and n_{a2} is the number of diagonal regions that differ by 2 bits from a type *a* symbol. Also, n_{b1I}, n_{b1Q}, n_{b2}, n_{c1I}, n_{c1Q}, n_{c2} are defined similarly for type *b* and type *c* symbols.

The bit error probability is thus

$$P_{ber} = \frac{1}{16}\left(n_a P_a + n_b P_b + n_c P_c\right) \quad \textbf{(21)}$$

where n_a, n_b, n_c is the number of *a*, *b*, *c* type regions in the constellation. For the 16-QAM case we can see that $n_a = 4, n_b = 8, n_c = 4$.

$$P_{ber} = \frac{1}{16}\left(4P_a + 8P_b + 4P_c\right) \quad \textbf{(22)}$$

By substituting values from Eq. (18) – (20) into the above equation, we get

$$P_{ber} = \frac{1}{16}\left(5P_{1I} + 7P_{1Q} + 18P_2\right) \quad \textbf{(23)}$$

$$= \frac{5}{16}Q\left[\frac{\sqrt{2}A\left(\alpha_I - \alpha_Q\right)}{\sqrt{N_w}}\right] + \frac{7}{16}Q\left[\frac{\sqrt{2}A\left(\alpha_I + \alpha_Q\right)}{\sqrt{N_w}}\right]$$

$$+ \frac{18}{16}Q\left[\frac{\sqrt{2}A\left(\alpha_I - \alpha_Q\right)}{\sqrt{N_w}}\right]Q\left[\frac{\sqrt{2}A\left(\alpha_I + \alpha_Q\right)}{\sqrt{N_w}}\right] \quad \textbf{(24)}$$

Denote $X = \alpha_I - \alpha_Q$ and $Y = \alpha_I + \alpha_Q$ with probability density function PDF given by Eq. (7) and Eq. (8). The bit error probability can be expressed as

$$P_b(X,Y) = \frac{5}{16}Q\left[\frac{\sqrt{2}A\,X}{\sqrt{N_w}}\right] + \frac{7}{16}Q\left[\frac{\sqrt{2}AY}{\sqrt{N_w}}\right] + \frac{18}{16}Q\left[\frac{\sqrt{2}A\,X}{\sqrt{N_w}}\right]Q\left[\frac{\sqrt{2}AY}{\sqrt{N_w}}\right] \quad \textbf{(25)}$$

The expectation of $P_b(x,y)$ gives the average bit error probability $\overline{P}_b$ and applying the same procedure as with QPSK modulation in the previous sub-section we have

$$P_b(Y) = \frac{5}{32} + Q\left(\frac{\sqrt{2}AY}{\sqrt{N_w}}\right) \quad \textbf{(26)}$$

$$\overline{P}_b = E[P_b(Y)] = \frac{5}{32} + Q\left(\frac{\mu}{\sqrt{1+\lambda^2}}\right) \quad \textbf{(27)}$$

where $\lambda = \frac{\sqrt{2}A\sigma}{\sqrt{N_w}}$, $\mu = \frac{\sqrt{2}Am_Y}{\sqrt{N_w}}$

The simulation results in Figure 4 show the theoretical and simulated results of non-coherent detection using QPSK and 16-QAM. As you can see the simulated BER curve is virtually flat showing the harsh nature of the dispersive channel and the theoretical BER curve agrees closely with it.

4. Construction of LDPC Codes using BIBD

LDPC codes are broadly classified by their method of construction: Random and Structured. Random codes are constructed using a random computer search based on certain design rules or graph structures, such as girth[†] and degree distribution whereas structured codes are based on algebraic or combinatoric methods. The method presented here is based on the construction of structured LDPC codes known as the balance incomplete block (BIBD) design. These LDPC codes have a girth of at least 6 and are cyclic, which consequently simplifies the encoding procedure compared with non-cyclic or quasi-cyclic LDPC codes.

As shown in [12] [19] the codes constructed using the structured method perform as closely or even better than randomly constructed codes e.g. MacKay codes. For example, an LDPC (2175, 2535) code

[†] The length of the cycle is the number of edges it contains, and the *girth* of a graph is the size of the smallest cycle.

used in this paper outperforms the equivalent Mackay code at a BER of 10^{-4} [12]. Another new LDPC-BIBD code of length 4351 and rate 0.947 has been generated and the BER has been simulated over the BFWA channel.

Another main advantage of using BIBD codes over randomly constructed LDPC codes is their lower encoding complexity. Whereas, quasi-cyclic LDPC codes like those generated by the BIBD design have an encoding advantage over random LDPC codes as they can be encoded using simple shift registers with complexity linearly proportional to their code length. For example in [20], Li *et al* shows that in order to implement the generator matrix of dimension 512 × 512 using quasi-cyclic structure requires 1024 flip-flops, 512 two-input AND gates and 512 two-input XOR gates, whereas the construction of the same size random generator matrix requires about 262144 two-input AND gates and 261632 two-input XOR gates.

4.1. Combinatorial Design

Combinatorial mathematics [10] basically deals with the theory of enumeration, permutation, combination and the arrangement of objects in order to satisfy certain conditions. Informally, one may define a combinatorial design to be a way of selecting subsets from a finite set in such a way that some specified conditions are satisfied. The detail of the construction of LDPC codes are well documented in [17], [18] and [19]. The detailed study of combinatorial mathematics shows that the parity check matrix **H** can be constructed using BIBD having covalency $\lambda = 1$. The covalency condition $\lambda = 1$ ensures the code is free of cycles of length 4 and results in a girth of at least 6. The example in Appendix B describes the relationship between LDPC codes and BIBD design.

Over the years many BIBD designs have been constructed and they are represented by mathematical equations so that variable length designs with different parameters can be constructed with ease. In this paper, we have selected the Bose BIBD design method [11], [12] to generate high rate LDPC codes.

4.2 Bose BIBD Design Example

Bose constructed many classes of BIBD design. The following example shows one of the types of Bose-BIBD design.

Let t be a positive integer that satisfies $12t + 1 = p$, where p is a prime number. There exists a Galois Field GF $(12t+1)$ with $12t + 1$ elements. Suppose GF $(12t+1)$ has a primitive root, x, such that $x^{4t} - 1 = x^c$, where c is an odd integer less than $12t+1$. Then there exists a BIBD design with the following parameters:

No of rows,	$v = 12t + 1$, Objects
No of columns,	$b = t\,(12t+1) = tv$, Blocks
Column weight,	$\gamma = 4$,
Row weight,	$\rho = \gamma t$
Covalency,	$\lambda = 1$

The design block is generated using the building blocks $B_i = \{0, x^{2i}, x^{2i+4t}, x^{2i+8t}\}$ for $0 \le i < t$. From B_i we can form $12t+1$ blocks by adding each element in the Galois Field GF $(12t+1)$. The incident matrix of this BIBD is a $(12t + 1) \times t\,(12t+1)$ matrix. It can be written in cyclic form consisting of t, $(12t + 1) \times (12t + 1)$ circulant sub matrices as follows:

$$\mathbf{Q} = [\mathbf{Q_1}, \mathbf{Q_2}, \ldots\ldots\ldots, \mathbf{Q_t}] \quad \textbf{(28)}$$

The incident matrix of Bose-BIBD consists of a row of t circulants. For $1 \le z \le t$ the parity check matrix is

$$\mathbf{H}\,[z] = [\mathbf{Q_1}, \mathbf{Q_2}, \ldots\ldots \mathbf{Q_z}] \quad \textbf{(29)}$$

Appendix C shows the incident matrix generation using the above method for t=1.

The advantage of BIBD scheme is that we can generate very high rate LDPC codes, which can be used to increase the bandwidth efficiency of the overall system. A number of new codes have been generated and the simulation section includes results using the newly designed (4351, 4123) LDPC code of rate 0.948.

5. Equalisation and LDPC Decoding

Time domain equalisers are usually of the transversal filter type (i.e. a tapped delay line filter) with coefficient values adjusted to minimise some error criterion. An automatic equalisation process requires an initial training period during which the equaliser reduces the error. In this paper we have used the square root Kalman (SRK) algorithm to adaptively determine the equaliser coefficients, which is an enhanced version of the recursive least square (RLS) algorithm.

5.1. Recursive least-square (RLS) algorithm

The Least Mean Square (LMS) algorithm is the simplest and most universally applicable adaptive algorithm [13]. This algorithm is important because of its simplicity, ease of computation, and because it does not require off-line gradient estimations or repetition of data. However, the price paid for its simplicity is slow convergence, especially when the channel characteristics result in an autocorrelation matrix ($\mathbf{\Gamma}$) whose eigenvalues have a large spread, i.e. $\lambda_{\max}/\lambda_{\min}$ >>1, where $\lambda_{\max}$ and $\lambda_{\min}$ are maximum and minimum eigenvalues respectively.

In deriving faster converging algorithms, a least squares (LS) approach is more appropriate. An important feature of the LS algorithm [14] is the utilisation of information contained in the input data, extending back to the instant of time when the algorithm was initiated. This results in faster convergence but at the cost of an increase in computational complexity.

The transmitted signal corrupted by Gaussian noise and ISI, r_n , arrives at the receiver. The receiver will then apply equalisation and decoding schemes to extract the transmitted bits, b_k,. The adaptive equaliser chosen for this application has 5 feed-forward and 3 feedback filter taps as shown in Figure 3. The vector containing the complex coefficients of` the filters is defined as $\mathbf{c}=[\mathbf{c}_0\ \mathbf{c}_1\ \mathbf{c}_2\ \mathbf{c}_3\ \mathbf{c}_4\ \mathbf{b}_0\ \mathbf{b}_1\ \mathbf{b}_2\ ]^{\mathrm{T}}$, and the input signal vector is defined as $\boldsymbol{r}_n=[\mathbf{r}_n\ \ \mathbf{r}_{n-1}\ \mathbf{r}_{n-2}\ \ \mathbf{r}_{n-3}\ \ \mathbf{r}_{n-4}\ \ \mathbf{d}_{n-1}\ \ \mathbf{d}_{n-2}\ \ \mathbf{d}_{n-3}\ \ ]^{\mathrm{T}}$ where ^{T} represents

matrix transposition, *d* represents the output of the decision device and *n* represents the discrete time instant.

Then the output $\mathbf{y_n}$ of the equalizer is given as

$$\mathbf{y_n} = \mathbf{c}\,\mathbf{r_n} \tag{30}$$

The error signal e_n can be formed as follows:

$$\mathbf{e_n} = \mathbf{d_n} - \mathbf{y_n} \tag{31}$$

During the training period, $\mathbf{d_n}$ is the training sequence and while receiving data, it is the output of the decision device (decision directed mode). The aim of the adaptive equalizer is to adjust the filter coefficients to move away from the initial condition mean squared error (ICMSE) towards the minimum mean squared error (MMSE).

The RLS algorithm requires that the initial values of the inverse correlation matrix $\mathbf{\Lambda_n}$ ensure the non-singularity of the correlation matrix $\mathbf{\psi_n}$ [14]. The coefficients are controlled by the Kalman gain vector resulting in rapid convergence compared to that of the LMS algorithm. But this RLS algorithm has the disadvantage of numerical instability. In order to tackle this problem, the RLS algorithm is modified to give the Square Root Kalman (SRK) or Square Root RLS algorithm.

5.2. Square Root Kalman (SRK) Algorithm

The problem with the RLS algorithm is that the update formula does not guarantee $\mathbf{\Lambda_n}$ is a positive definite matrix [15]. The SRK algorithm overcomes the problem by performing a U-D factorization of the matrix such that

$$\mathbf{\Lambda_n} = \mathbf{U_n^*}\,\mathbf{D_n}\,\mathbf{U_n^T}, \tag{32}$$

where $\mathbf{U_n}$ is an upper triangular matrix and $\mathbf{D_n}$ is a diagonal matrix. The time updating is carried out on the matrices $\mathbf{U_n}$ and $\mathbf{D_n}$. The procedure of finding the recursive update of $\mathbf{\Lambda_n}$ is defined in [15]. This paper also describes the computational procedures to carry out the square root formulation.

5.3. LDPC Decoding

For our simulation the equaliser is trained initially by using 200 training symbols and then goes into decision directed mode. The equalized output is then subsequently demodulated/de-interleaved and the log-likelihood ratios are passed to the LDPC decoder to extract the information bits.

Let $x_{i,1}$ and $x_{i,2}$ represent the two bits of a QPSK symbol. The LLR for the first bit of the symbol x_1 can be written as

$$\ln\left(\frac{P\left(x_{1,1}=1\right)}{P\left(x_{1,1}=0\right)}\right)=\ln\left(\frac{\sum_{j=0,3}P\left(x_1=s_j\mid c\right)}{\sum_{j=1,2}P\left(x_1=s_j\mid c\right)}\right) \tag{33}$$

Similarly, for second bit of the symbol x_1

$$\ln\left(\frac{P\left(x_{1,2}=1\right)}{P\left(x_{1,2}=0\right)}\right)=\ln\left(\frac{\sum_{j=0,1}P\left(x_1=s_j\mid c\right)}{\sum_{j=2,3}P\left(x_1=s_j\mid c\right)}\right) \tag{34}$$

where c is the output from the de-interleaver and s_j is the j^{th} QPSK symbol. This procedure can be extended to higher modulation schemes such as QAM. These likelihood ratios are then exchanged between the check and variable nodes of the LDPC code. The connections between these nodes are formed according to the position of 1's in the parity check matrix **H**. The number of internal iterations was set to 7 in this case. The exchange of information between variable and check nodes is explained as follows:

The variable node of the decoder facing towards the channel receives the reliability information in the form of Log-likelihood ratios (LLR). The variable node edges of the tanner graph connected to the check nodes are initialized to these reliability values. So, these messages are passed to the

corresponding check nodes for the extrinsic log-likelihood calculations. The calculations at one particular check node are based on the product of the information from the other variable nodes excluding the one that particular check node is directly connected to. These extrinsic log likelihood values calculated at the check nodes are now being passed back to the variable nodes. So these new messages in the form of LLRs at variable nodes are summed together with the original LLR (from the channel) and then the parity check is applied to check that it satisfies the syndrome equation. If the parity check fails then the new LLRs (or messages) at the variable nodes are generated for the next iteration and passed on to the corresponding check nodes for extrinsic information. At a particular variable node, the calculations of new the updated LLR to be passed to the corresponding check node takes into account the messages (LLRs) from all the other check nodes not from the one it is directly connected to.

This exchange of information between variable and check node updates the original LLRs and at every iteration a parity check is applied to confirm the validity of the LLR update. This whole iterative process continues until the parity check satisfies the syndrome equation $\mathbf{c}^{\mathbf{T}} \cdot \mathbf{H} = \mathbf{0}$ or the maximum iteration is reached. Hence, in this algorithm at the check node the extrinsic information is based on the product of LLRs passed from variable nodes and at the variable node the new information is based on the summation of the updated extrinsic information from the check node and the original LLR.

6. Analysis of Simulation Results

The simulation results presented here use LDPC codes constructed using the BIBD design method. Two different codes were compared; the (2715, 2535) LDPC-BIBD code (rate 0.933) and a newly designed (4351, 4123) LDPC-BIBD with rate of 0.948. The LDPC codes are free of cycle four and the LDPC decoder utilizes the message passing algorithm to decode the information bits. The maximum number of decoder iterations in all simulations is set to 10, since experiments showed that negligible

additional coding gain was achieved when iterations greater than 10 were performed. The simulation results shown in Figure 5 and 6 shows the performance of (2715, 2535) LDPC-BIBD and (4351, 4123) LDPC-BIBD over the AWGN and Rayleigh fading channel respectively. The figure shows the strength of these high rate codes compared to uncoded QPSK BER curve over AWGN and Rayleigh fading channel.

These codes are tested using QPSK and 16-QAM modulation schemes (gray coded) over a channel simulated by the SUI-3 BFWA model. As mentioned earlier, the SUI-3 model consists of three taps with the first one Rician distributed and the others having Rayleigh distributions. This model includes tap delays of 0 μs, 0.5 μs and 1.0 μs, with relative powers 0 dB, -5 dB and -10 dB, and with K-factor 1, 0 and 0, respectively. The Doppler spread is 0.4 Hz and the delay spread is 0.264 μs.

Figure 7 compares the performance of the (2715, 2535) LDPC-BIBD code using equalisation and OFDM transmission scheme having 256 sub-carrier with QPSK modulation. The most immediate observation is that without equalisation, the ISI dominates the performance and the LDPC coding alone provides negligible gain over uncoded QPSK, in contrast to its very promising performance over the AWGN channel. A small improvement in performance over the uncoded system can be achieved using either equalisation or OFDM, with SRK equalisation slightly outperforming OFDM, but both schemes suffer from an error floor. By including the LDPC code the error floor is 'broken' and significant coding gains are achieved over the uncoded equalised and OFDM systems. The results show that the LDPC code with SRK equalisation outperforms the scheme with the LDPC code and OFDM on the BFWA channel, particularly at lower signal-to-noise ratios, with a coding gain of around 1dB at a BER = 10^{-3}.

Figure 8 shows the simulation results of the (4351, 4123) LDPC-BIBD code using equalisation and OFDM with QPSK over the BFWA channel. Once again, this longer code still does not perform well

over the BFWA channel on its own and when used with SRK equalisation has approximately 1 dB coding gain at a BER = 10^{-3} over the OFDM system.

Figure 9 and Figure 10 show the performance comparison of the (2715, 2535) and (4351, 4123) LDPC codes respectively using equalisation and OFDM with 16-QAM over the BFWA channel. The receiver performance using LDPC coding on its own is again plotted for reference. With OFDM transmission we find the BER performance is again vastly improved. However, if we compare the equalised system with the OFDM system for the same code length, the SRK equalisation scheme performs slightly better then OFDM scheme with an improvement of approximately 1 dB at BER 10^{-3}.

7. Conclusion

In this paper, high rate variable length LDPC codes have been constructed using the BIBD method and their performance over the BFWA channel has been evaluated with SRK equalisation and OFDM modulation separately to overcome the ISI introduced by the channel. The BFWA channel is very harsh and without either of these techniques the LDPC codes perform poorly. The theoretical analysis of BFWA channel with a non-coherent detection technique matches closely with the results obtained by simulations using QPSK/16-QAM. The simulation results show that significant coding gains can be achieved using LDPC codes with SRK equalisation or OFDM over uncoded systems. However, LDPC codes with SRK equalisation do outperform LDPC codes with OFDM over the BFWA channel, particularly at lower signal-to-noise ratios. The performance is worse when using OFDM since it reduces what little frequency diversity is available in the BFWA channel resulting in the LDPC code being unable to effectively recover this lost diversity. Consequently, for a single carrier with SRK equalisation we can still take advantage of more of the available channel frequency diversity. Also, the use of high rate LDPC codes and high constellation QAM will minimise bandwidth use and improve

the overall data rate of the system. Future work will be to investigate joint equalisation and LDPC decoding to improve the performance over the Multi-Input-Multi-Output (MIMO) BFWA channel.

Acknowledgment

The authors wish to thank the EPSRC for their financial support of this research.

Appendix A

According to equation (10) in section 3.1.1, we have

$$P_b(X,Y)=\frac{1}{2}Q\left(\frac{X}{\sqrt{N_w}}\right)Q\left(\frac{-Y}{\sqrt{N_w}}\right)+\frac{1}{2}Q\left(\frac{-X}{\sqrt{N_w}}\right)Q\left(\frac{Y}{\sqrt{N_w}}\right)+Q\left(\frac{X}{\sqrt{N_w}}\right)Q\left(\frac{Y}{\sqrt{N_w}}\right)$$

where *X* and *Y* are defined as $X=\mathrm{Re}\{\alpha_o\}-\mathrm{Im}\{\alpha_0\}$ and $Y=\mathrm{Re}\{\alpha_o\}+\mathrm{Im}\{\alpha_0\}$. In fact, the bit error probability is not only a function of *x* and *y*, but also a function of $A_1=|\alpha_1|^2$ and, $A_2=|\alpha_2|^2$ i.e.,

$$P_b(X,Y,A_1,A_2)=\frac{1}{2}Q\left(\frac{X}{\sqrt{A_1+A_2+N_0}}\right)Q\left(\frac{-Y}{\sqrt{A_1+A_2+N_0}}\right)$$
$$+\frac{1}{2}Q\left(\frac{-X}{\sqrt{A_1+A_2+N_0}}\right)Q\left(\frac{Y}{\sqrt{A_1+A_2+N_0}}\right)+Q\left(\frac{X}{\sqrt{A_1+A_2+N_0}}\right)Q\left(\frac{Y}{\sqrt{A_1+A_2+N_0}}\right) \quad \textbf{(35)}$$

For a specific data block, the channel coefficients $\alpha_0,\alpha_1,\alpha_2$ are fixed and the bit error rate of this specific data block can be computed by (35) provided that the channel coefficients are known. However, the aim of this analysis is to derive the bit error probability averaged over many data blocks, where the channel coefficients vary from block to block. The average P_b, denoted as $\overline{P_b}$ is derived by averaging $P_b(X,Y,A_1,A_2)$ over the distribution of x, y, A_1, A_2, i.e,

$$\overline{P_b}=\int_0^\infty\int_0^\infty\int_{-\infty}^\infty\int_{-\infty}^\infty P_b(X,Y,A_1,A_2)p(X)\,p(Y)\,p(A_1)\,p(A_2)\,dX\,dY\,dA_1\,dA_2 \quad \textbf{(36)}$$

where, $p(X), p(Y), p(A_1), p(A_2)$ are the PDF functions of X, Y, A_1, A_2, respectively. In the derivation of the average bit error rate, X, Y, A_1, A_2 should be viewed as random variables since they differ from one block to another.

The amplitude of α_0, i.e., $|\alpha_0|^2$ is characterized by a Ricean distribution [3] due to line-of-sight propagation (the real and imaginary parts of α_0, are non-zero mean Gaussian random variables), *X* and *Y* are still Gaussian distributed with PDFs defined by (7) and (8). Also, $|\alpha_1|$ and $|\alpha_2|$ are characterized by a Rayleigh distribution [3] due to non-line-of-sight propagation (both real and imaginary parts of α_1 and α_2 are zero mean Gaussian random variables). Therefore, each of the random variables A_1 and A_2 has a central chi-square distribution with 2 degrees of freedom and PDF [22]

$$p(A_1) = \frac{1}{\gamma_1}\exp\left[-\frac{A_1}{\gamma_1}\right], \qquad A_1 \geq 0$$
$$p(A_2) = \frac{1}{\gamma_2}\exp\left[-\frac{A_2}{\gamma_2}\right], \qquad A_2 \geq 0 \tag{37}$$

where, $\gamma_1 = P_1 = E[A_1] = E\left[|\alpha_1|^2\right]$, and $\gamma_2 = P_2 = E[A_2] = E\left[|\alpha_2|^2\right]$. Substituting (7), (8) and (37) into (36), we obtain

$$\overline{P_b} = \frac{1}{2\pi\sigma^2\gamma_1\gamma_2}\int_{-\infty}^{\infty}\int_{-\infty}^{\infty}\int_{0}^{\infty}\int_{0}^{\infty} P_b(X, Y, A_1, A_2)\exp\left[-\frac{X^2}{2\sigma^2}\right]\exp\left[-\frac{(Y-m_Y)^2}{2\sigma^2}\right]$$
$$\exp\left[-\frac{A_1}{\gamma_1}\right]\exp\left[-\frac{A_2}{\gamma_2}\right]dX\,dY\,dA_1\,dA_2 \tag{38}$$

The exact average bit error probability for the QPSK modulated BFWA system should be calculated with Eq. (38). However, the derivation of its closed form expression does not seem to be tractable, and numerical evaluation of this four-fold integral would be too tedious. In what follows, we obtain a closed form formula for average bit error probability by using some approximation methods. One

simplification measure is to remove the dependence of A_1, A_2 in (35) by taking the expectation with respect to random variables A_1, A_2

$$E\left[P_b(X,Y,A_1,A_2)\right] = P_b(X,Y)$$
$$\approx \frac{1}{2}Q\left(\frac{X}{\sqrt{N_w}}\right)Q\left(\frac{-Y}{\sqrt{N_w}}\right) + \frac{1}{2}Q\left(\frac{-X}{\sqrt{N_w}}\right)Q\left(\frac{Y}{\sqrt{N_w}}\right) + Q\left(\frac{X}{\sqrt{N_w}}\right)Q\left(\frac{Y}{\sqrt{N_w}}\right) \quad \textbf{(39)}$$

The approximation in (39) is due to the fact that instead of carrying out integration to evaluate expectation, we simply replace the noise plus interference term $N_{ISI+noise} = A_1 + A_2 + N_0$ with its mean value $E\left[N_{ISI+noise}\right] = N_w = P_1 + P_2 + N_0$. This is so-called standard Gaussian approximation (GA) in the literature. An example is shown in [23] (see equations (25), (26)). The exact analysis is carried out by equation (41) in [23]. By comparison, one can see that the random variable ψ (i.e., the MAI variance) in [23, Eq (41)] is replaced by its mean value $E[\psi] = E\left[\sum_{k=2}^{K} Z_k\right] = (K-1)N/3$ in [23, Eq (25)] and [23, Eq (26)] so that the integration expressed by [23, Eq (41)] can be avoided. It has been shown in [23], [24] that this approximation method gives close results to that derived by the exact analysis using integrations at high bit error rate. Therefore, it is well-suited to the performance analysis of the non-coherent detection scheme for which the performance is usually poor (bit error rate is high). It was also concluded in [23], [24] that this approximation method generally gives optimistic results. This concurs with our results shown in Fig. 4, where we can observe that theoretical curves lie below the simulation curves for both QPSK and 16-QAM systems.

A more accurate and still simple approximation method to evaluate expectation without carrying out integration was proposed by Holtzman in [25]. It was shown that the accuracy of analysis can be improved if not only the first order statistic (mean value), but also the second order statistic (variance) of the random variable is taken into account. In our case, it means we not only use E[A_1] and E[A_2],

but also var[A_1] and var[A_2] in the calculation of $P_b(x, y)$. Holtzman approximation has been adopted in several papers, e.g., in [26] for analysis of CDMA systems with parallel interference cancellation scheme and in [27] for analysis of the BFWA system with coherent detection. However, this approach is not considered here because the target system to be analyzed is the BFWA system with non-coherent detection, for which the bit error rate is high, and in such a scenario, standard GA gives sufficient accuracy as indicated in [23], [24].

$$\overline{P_b} = \int_{-\infty}^{\infty}\int_{-\infty}^{\infty} P_b(X,Y)p(X)\,p(Y)dX\,dY \qquad \textbf{(40)}$$

where $P_b(X,Y)$ is given by (39). Next, it is shown how the above integral can be avoided by using the fact that both *X* and *Y* are Gaussian random variables and by utilizing some properties of the *Q*-function given its arguments are Gaussian random variables. Since *x* is a zero-mean Gaussian random variable, $E[Q(\lambda x)] = Q(0) = 0.5$ [28, p. 102]. Therefore, expectation of (39) with respect to *x* is equivalent to

$$P_b(Y) \approx \frac{1}{4}Q\left(\frac{-Y}{\sqrt{N_w}}\right) + \frac{3}{4}Q\left(\frac{Y}{\sqrt{N_w}}\right) \qquad \textbf{(41)}$$

which is equivalent to Eq. (11)

Appendix B

BIBD Design Example

Let O = $\{x_1, x_2, x_3, x_4, x_5, x_6, x_7\}$ be a set of seven objects. The following blocks:

$\{x_1, x_2, x_4\}$, $\{x_2, x_3, x_5\}$, $\{x_3, x_4, x_6\}$, $\{x_4, x_5, x_7\}$, $\{x_5, x_6, x_1\}$, $\{x_6, x_7, x_2\}$, $\{x_7, x_1, x_3\}$

form BIBD for the set O. The parameters of the BIBD design are as follows:

No of objects; $v = 7$

No of blocks; $b = 7$

The block consists of three objects, each object appears in three blocks and every object appears together in pairs in exactly one block, *i.e.* covalency $\lambda = 1$. The incident matrix **Q** of this BIBD is given as follows:

$$\mathbf{Q} = \begin{bmatrix} 1 & 0 & 0 & 0 & 1 & 0 & 1 \\ 1 & 1 & 0 & 0 & 0 & 1 & 0 \\ 0 & 1 & 1 & 0 & 0 & 0 & 1 \\ 1 & 0 & 1 & 1 & 0 & 0 & 0 \\ 0 & 1 & 0 & 1 & 1 & 0 & 0 \\ 0 & 0 & 1 & 0 & 1 & 1 & 0 \\ 0 & 0 & 0 & 1 & 0 & 1 & 1 \end{bmatrix}$$

The rows are the right cyclic shifts of the row above and columns are the downward cyclic shifts of the last column. **Q** is known as a 7×7 square circulant matrix or circulant. Therefore, BIBD with $\lambda = 1$ has all the structural properties of the LDPC parity check matrix.

Appendix C

Example of Bose BIBD design *t*= 1

BIBD Bose parameters will be as follows

GF (12 +1) = GF (13), prime number $p = 13$

No of rows, $v = 13$, *Objects*

No of columns, $b = t\ v = 13$, *blocks*

Column weight, $\gamma = 4$,

Row weight, $\rho = 4 \times 1 = 4$,

Primitive Root of GF(13) , $x = 2$

$Bi = (0, x^{2i}, x^{2i+4t}, x^{2i+8t})$ for $0 \leq i < t$

$B_0 = (0, 2^0, 2^4, 2^8)$, for $i = 0$

$B_0 = (0, 1, 3, 9)$, for $i = 0$

B_0 is one of the blocks of GF (13), the other 12 blocks can be obtained by adding all the elements of GF (13) to B_0.

Blocks of Incident Matrix:

$$
\begin{aligned}
B_0 &\quad (0, 1, 3, 9) + 0 = (0, 1, 3, 9)\\
B_1 &\quad (0, 1, 3, 9) + 1 = (1, 2, 4, 10)\\
B_2 &\quad (0, 1, 3, 9) + 2 = (2, 3, 5, 11)\\
B_3 &\quad (0, 1, 3, 9) + 3 = (3, 4, 6, 12)\\
B_4 &\quad (0, 1, 3, 9) + 4 = (4, 5, 7, 0)\\
B_5 &\quad (0, 1, 3, 9) + 5 = (5, 6, 8, 1)\\
B_6 &\quad (0, 1, 3, 9) + 6 = (6, 7, 9, 2)\\
B_7 &\quad (0, 1, 3, 9) + 7 = (7, 8, 10, 3)\\
B_8 &\quad (0, 1, 3, 9) + 8 = (8, 9, 11, 4)\\
B_9 &\quad (0, 1, 3, 9) + 9 = (9, 10, 12, 5)\\
B_{10} &\quad (0, 1, 3, 9) + 10 = (10, 11, 0, 6)\\
B_{11} &\quad (0, 1, 3, 9) + 11 = (11, 12, 1, 7)\\
B_{12} &\quad (0, 1, 3, 9) + 12 = (12, 0, 2, 8)
\end{aligned}
$$

The incident matrix **Q** can be obtained by setting '1' in the position specified by each block as shown below.

$$
\begin{array}{c|cccccccccccc}
 & B_0 & B_1 & B_2 & B_3 & B_4 & B_5 & B_6 & B_7 & B_8 & B_9 & B_{10} & B_{11} & B_{12} \\
\hline
 & \mathbf{1} & \mathbf{0} & \mathbf{0} & \mathbf{0} & \mathbf{1} & \mathbf{0} & \mathbf{0} & \mathbf{0} & \mathbf{0} & \mathbf{0} & \mathbf{1} & \mathbf{0} & 1 \\
 & \mathbf{1} & \mathbf{1} & \mathbf{0} & \mathbf{0} & \mathbf{0} & \mathbf{1} & \mathbf{0} & \mathbf{0} & \mathbf{0} & \mathbf{0} & \mathbf{0} & \mathbf{1} & 0 \\
 & \mathbf{0} & \mathbf{1} & \mathbf{1} & \mathbf{0} & \mathbf{0} & \mathbf{0} & \mathbf{1} & \mathbf{0} & \mathbf{0} & \mathbf{0} & \mathbf{0} & \mathbf{0} & 1 \\
 & \mathbf{1} & \mathbf{0} & \mathbf{1} & \mathbf{1} & \mathbf{0} & \mathbf{0} & \mathbf{0} & \mathbf{1} & \mathbf{0} & \mathbf{0} & \mathbf{0} & \mathbf{0} & 0 \\
 & \mathbf{0} & \mathbf{1} & \mathbf{0} & \mathbf{1} & \mathbf{1} & \mathbf{0} & \mathbf{0} & \mathbf{0} & \mathbf{1} & \mathbf{0} & \mathbf{0} & \mathbf{0} & 0 \\
 & \mathbf{0} & \mathbf{0} & \mathbf{1} & \mathbf{0} & \mathbf{1} & \mathbf{1} & \mathbf{0} & \mathbf{0} & \mathbf{0} & \mathbf{1} & \mathbf{0} & \mathbf{0} & 0 \\
v = 13 & \mathbf{0} & \mathbf{0} & \mathbf{0} & \mathbf{1} & \mathbf{0} & \mathbf{1} & \mathbf{1} & \mathbf{0} & \mathbf{0} & \mathbf{0} & \mathbf{1} & \mathbf{0} & 0 \\
 & \mathbf{0} & \mathbf{0} & \mathbf{0} & \mathbf{0} & \mathbf{1} & \mathbf{0} & \mathbf{1} & \mathbf{1} & \mathbf{0} & \mathbf{0} & \mathbf{0} & \mathbf{1} & 0 \\
 & \mathbf{0} & \mathbf{0} & \mathbf{0} & \mathbf{0} & \mathbf{0} & \mathbf{1} & \mathbf{0} & \mathbf{1} & \mathbf{1} & \mathbf{0} & \mathbf{0} & \mathbf{0} & 1 \\
 & \mathbf{1} & \mathbf{0} & \mathbf{0} & \mathbf{0} & \mathbf{0} & \mathbf{0} & \mathbf{1} & \mathbf{0} & \mathbf{1} & \mathbf{1} & \mathbf{0} & \mathbf{0} & 0 \\
 & \mathbf{0} & \mathbf{1} & \mathbf{0} & \mathbf{0} & \mathbf{0} & \mathbf{0} & \mathbf{0} & \mathbf{1} & \mathbf{0} & \mathbf{1} & \mathbf{1} & \mathbf{0} & 0 \\
 & \mathbf{0} & \mathbf{0} & \mathbf{1} & \mathbf{0} & \mathbf{0} & \mathbf{0} & \mathbf{0} & \mathbf{0} & \mathbf{1} & \mathbf{0} & \mathbf{1} & \mathbf{1} & 0 \\
 & \mathbf{0} & \mathbf{0} & \mathbf{0} & \mathbf{1} & \mathbf{0} & \mathbf{0} & \mathbf{0} & \mathbf{0} & \mathbf{0} & \mathbf{1} & \mathbf{0} & \mathbf{1} & 1 \\
\hline
 & \multicolumn{13}{c}{b = 13}
\end{array}
$$

REFERENCES

[1] W.Webb. "Broadband fixed wireless access as a key component of the future integrated communication environment," *IEEE Communication Magazine*, vol. 39, pp. 115-121, Sept.2001.

[2] V. Erceg, K.V.S. Hari, M.S. Smith, D.S. Baum et al, "Channel Models for Fixed Wireless Applications", Contribution IEEE 802.16.3c-01/29r1, Feb. 2001.

[3] IEEE Standard, "Part 16: Air interface for fixed broadband wireless access systems – Amendment 2: Media access control modifications and additional physical layer specifications for 2-11 GHz," IEEE 802.16a, January 2003.

[4] G. L. Stuber, J. R. Barry, S. W. McLaughlin, Y. G. Li, M. A. Ingram, and T. G. Pratt, "Broadband MIMO-OFDM wireless communications," *Proceedings of the IEEE*, vol. 92, pp. 271–294, Feb.2004.

[5] T.J.Willink, "MIMO OFDM for broadband fixed wireless access," *IEE Proceedings on Communications,* vol. 12, issue 1, pp. 75-81, February 2005.

[6] C. Berrou, A. Glavieux, and P. Thitimajshima, "Near Shannon limit errorcorrecting coding and decoding: Turbo-codes," in *Conference Record, IEEE International Conference on Communications, ICC-93*, May 1993, vol. 2, pp. 1064.1070.

[7] S. Benedetto and G. Montorsi, "Unveiling turbo codes: some results on parallel concatenated coding schemes," *IEEE Transactions on Information Theory*, vol. 42, no. 2, pp. 409-428, March 1996.

[8] S. Benedetto, D. Divsalar, G. Montorsi, and F. Pollara, "Serial concatenation of interleaved codes: performance analysis, design, and iterative decoding," *IEEE Transactions on Information Theory*, vol. 44, no. 3, pp. 909-926, May 1998.

[9] R.G. Gallager, Low Density Parity-Check Codes. MIT Press, Cambridge, MA, 1963.

[10] I. F. Blake and R. Mullin, *The Mathematical Theory of Coding*. NewYork: Academic, 1975.

[11] R. C. Bose, "On the construction of balanced incomplete block designs," *Ann. Eugenics 9*, pp. 353–399, 1939.

[12] B.Ammar, B. Honary, "Construction of Low-Density Parity-Check Codes Based on Balance Incomplete Designs," in *IEEE Transaction on Information Theory,* vol.50, pp. 1257-1268, June 2004.

[13] Widrow, B. and Hoff, "Adaptive switching circuits, Institute of Radio Engineers," in W*ESCON Convention Record*, pages 96 – 104 August 1960.

[14] Haykin.S, "Adaptive filter theory," 3rd edition, Prentice Hall International Inc., 1996.

[15] Hsu.FM, "Square Root Kalman filtering for high-speed data received over fading dispersive HF channels," *IEEE Transaction on Information Theory,* vol. IT-28, No.5, September 1982.

[16] P.Xiao, R.A. Carrasco and I.J. Wassell, "Performance Analysis of Conventional Detection in BFWA Systems," In *Proc. Second IFIP International Conference on Wireless and Optical Communications Networks, WOCN'2005*, pp. 447-452, March 2005, Dubai, UAE.

[17] B. Vasic, and O. Milenkovic, "Combinatorial Constructions of Low-Density Parity-Check Codes for Iterative Decoding," *IEEE Trans. on Inform. Theory*, vol. 50, No. 6, June 2004.

[18] B. Vasic, E. Kurtas and A. Kuznetsov, "LDPC Codes Based on Mutually Orthogonal Latin Rectangles and their Application in Perpendicular Magnetic Recording," *IEEE Trans. Magnetics*, Vol. 38, No. 5, Part: 1, pp.2346 -2348, Sep. 2002.

[19] B. Honary. A. Moinian and B. Ammar, "Construction of Well-Structured Quasi-Cyclic Low Density Parity Check Codes," *IEE Proceedings on Communications*, vol. 152, no. 6, pp. 1081-1085, Dec. 2005.

[20] Z.W. Li, L.Chen, S. Lin and W. Fong, "Efficient encoding of quasi-cyclic low- density parity-check codes," *IEEE Trans. on Comms.,* vol. 54, No. 1, January 2006.

[21] P.Xiao, R.A. Carrasco and I.J. Wassell, "Theoretical Performance Analysis of Single and Multiple Antenna FWA Systems," Accepted for Publication in *IEE Proceedings of Communications*.

[22] J. Proakis. Digital Communications, 3rd edition, McGraw-Hill, 1995.

[23] R. Morrow and J. Lehnert, "Bit-to-bit error dependence in slotted DS/SSMA packet systems with random signature sequences,"*IEEE Transactions on Communications*, vol. 37, no. 10, pp. 1052-1061, Oct. 1989.

[24] R. Buehrer and B. Woerner, "Analysis of adaptive multistage interference cancellation for CDMA using an improved Gaussian approximation," *IEEE Transactions on Communications*, vol. 44, no. 10, pp. 1308-1321.

[25] J. Holtzman, "A simple, accurate method to calculate spread-spectrum multiple-access error probabilities," *IEEE Transactions on Communications*, vol. 40, no. 3, pp. 461-464, March 1992.

[26] P. Xiao, E. Strom, "A theoretical evaluation of parallel interference cancellation in M-ary orthogonal modulated asynchronous DS-CDMA system over multipath Rayleigh fading channels," IEEE Transactions on Vehicular Technology, vol. 54, no. 4, pp. 1400{1414, July, 2005.

[27] P. Xiao, R. Carrasco, I. Wassell, "Performance analysis of conventional detection in BFWA systems," Proc. Second IFIP International Conference on Wireless and Optical Communications Networks, pp. 447{452, March 2005.

[28] S. Verdu. Multiuser Detection, 1st edition, Cambridge University Press, 1998.

FIGURE CAPTIONS

Fig.1: The complete diagram of the single-input single-output LDPC coded BFWA system, (a) with equalisation (b) with OFDM.

Fig. 2: Constellation diagram of a coded (a) QPSK (b) 16-QAM

Fig. 3: Structure of Adaptive Equaliser using 5 feed-forward and 3 feedback taps

Fig. 4: Non-coherent detection of QPSK and 16-QAM over the BFWA channel.

Fig. 5: Performance of the (2715, 2535) LDPC code over the AWGN and Rayleigh Fading Channel

Fig. 6: Performance of the (4351, 4123) LDPC code over the AWGN and Rayleigh Fading Channel

Fig. 7: Comparison of Simulation results of the (2715, 2535) LDPC code using QPSK over the BFWA channel.

Fig. 8: Comparison of Simulation results of the (4351, 4123) LDPC code using QPSK over the BFWA channel.

Fig. 9: Comparison of Simulation results of (2715, 2535) LDPC code using QAM over the BFWA channel.

Fig. 10: Comparison of Simulation results of the (4351, 4123) LDPC code using QAM over the BFWA channel.

Figure 1

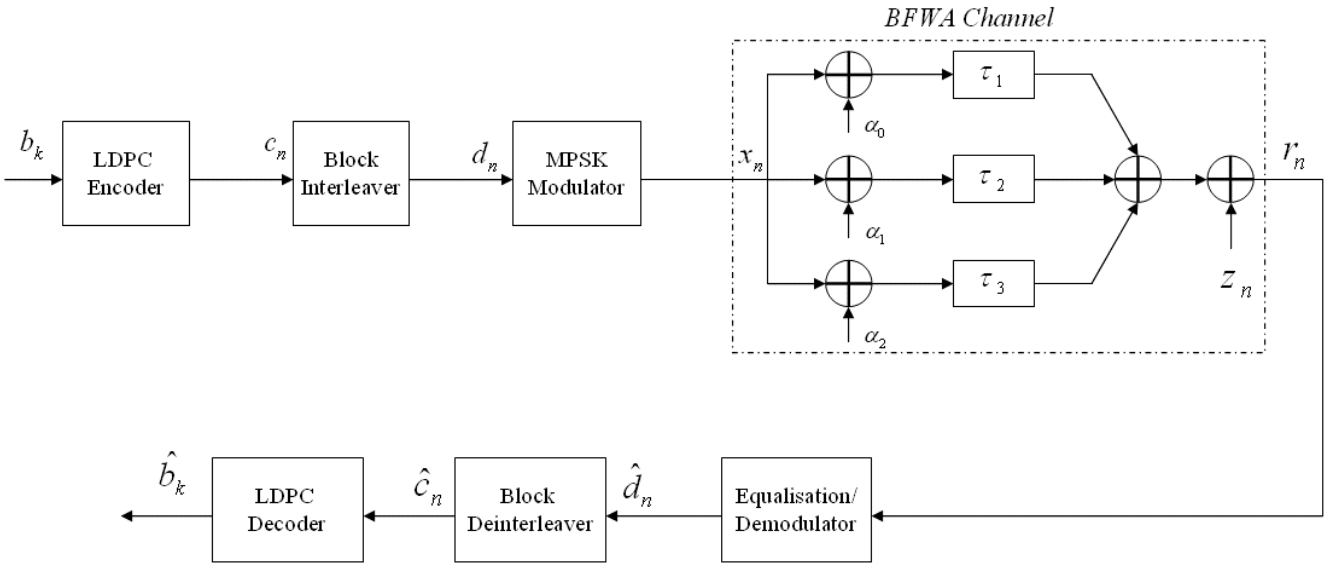
BFWA Channel
b_k
LDPC Encoder
c_n
Block Interleaver
d_n
MPSK Modulator
x_n
α_0
α_1
α_2
τ_1
τ_2
τ_3
z_n
r_n
$\hat{b}_k$
LDPC Decoder
$\hat{c}_n$
Block Deinterleaver
$\hat{d}_n$
Equalisation/ Demodulator

(a)

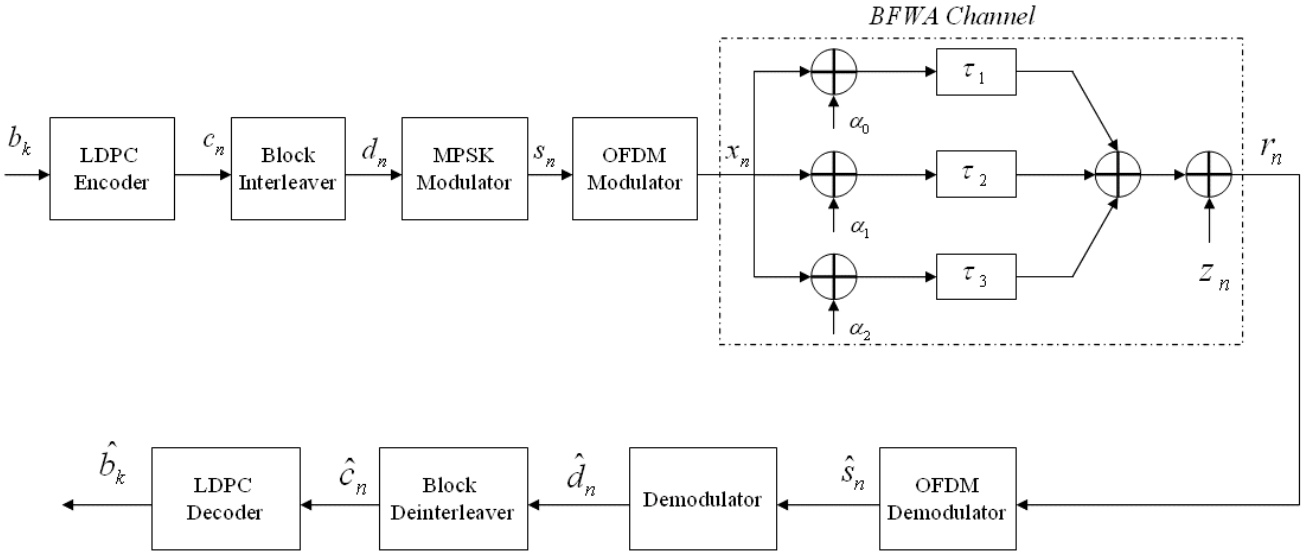
BFWA Channel
b_k
LDPC Encoder
c_n
Block Interleaver
d_n
MPSK Modulator
s_n
OFDM Modulator
x_n
α_0
α_1
α_2
τ_1
τ_2
τ_3
z_n
r_n
$\hat{b}_k$
LDPC Decoder
$\hat{c}_n$
Block Deinterleaver
$\hat{d}_n$
Demodulator
$\hat{s}_n$
OFDM Demodulator

(b)

Figure 2

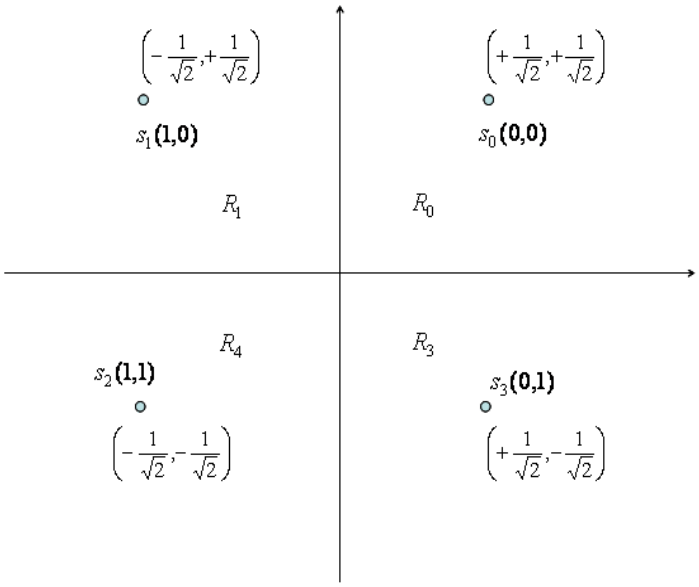
$\left(-\frac{1}{\sqrt{2}},+\frac{1}{\sqrt{2}}\right)$
$\left(+\frac{1}{\sqrt{2}},+\frac{1}{\sqrt{2}}\right)$
$s_1(1,0)$
$s_0(0,0)$
R_1
R_0
R_4
R_3
$s_2(1,1)$
$s_3(0,1)$
$\left(-\frac{1}{\sqrt{2}},-\frac{1}{\sqrt{2}}\right)$
$\left(+\frac{1}{\sqrt{2}},-\frac{1}{\sqrt{2}}\right)$

(a)

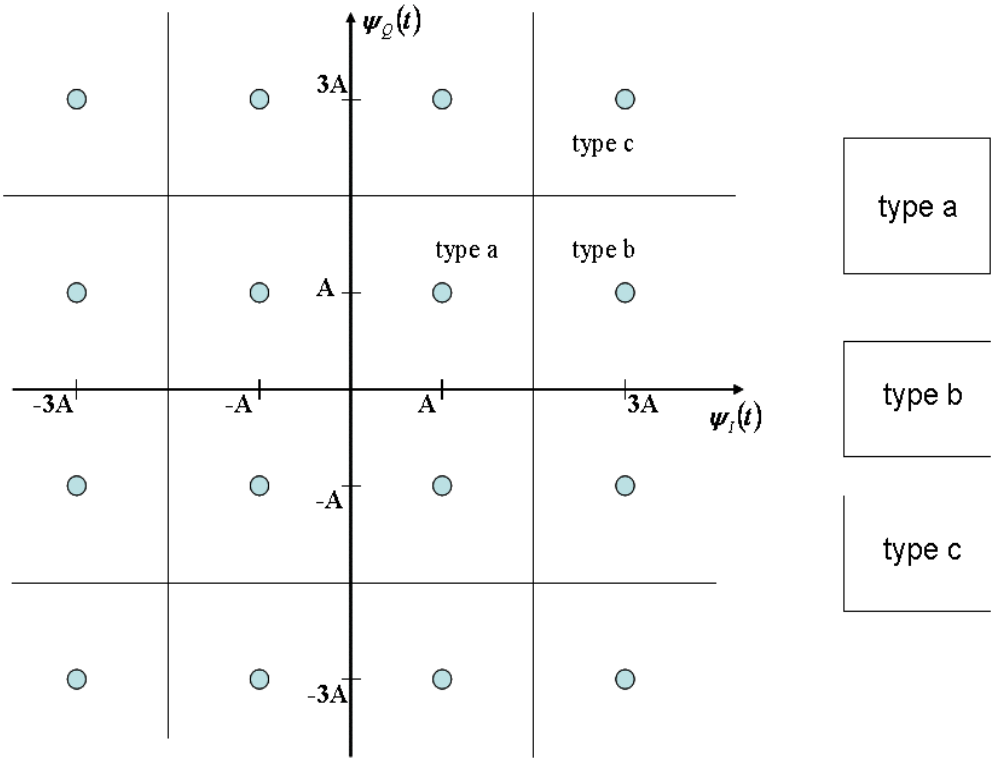
$\psi_Q(t)$
3A
A
-A
-3A
-3A
-A
A
3A
$\psi_I(t)$
type c
type a
type b
type a
type b
type c

(b)

Figure 3

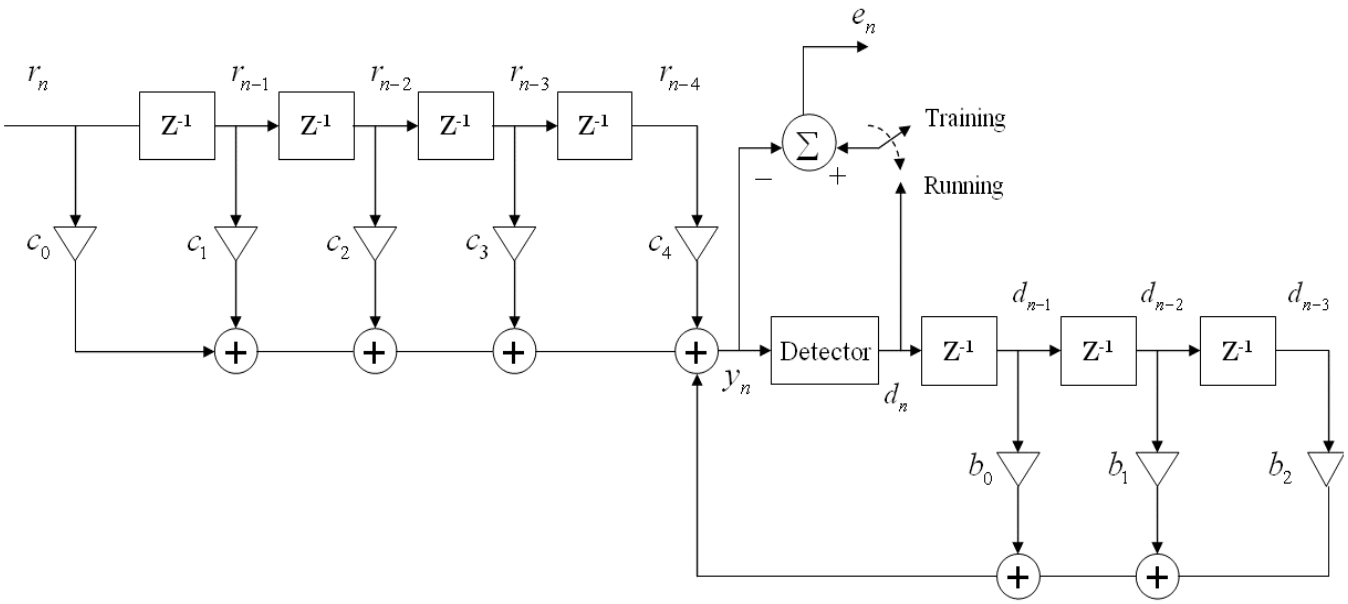
r_n
r_{n-1}
r_{n-2}
r_{n-3}
r_{n-4}
Z-1
Z-1
Z-1
Z-1
e_n
Σ
Training
Running
−
+
c_0
c_1
c_2
c_3
c_4
d_{n-1}
d_{n-2}
d_{n-3}
Detector
Z-1
Z-1
Z-1
y_n
d_n
b_0
b_1
b_2

Figure 4

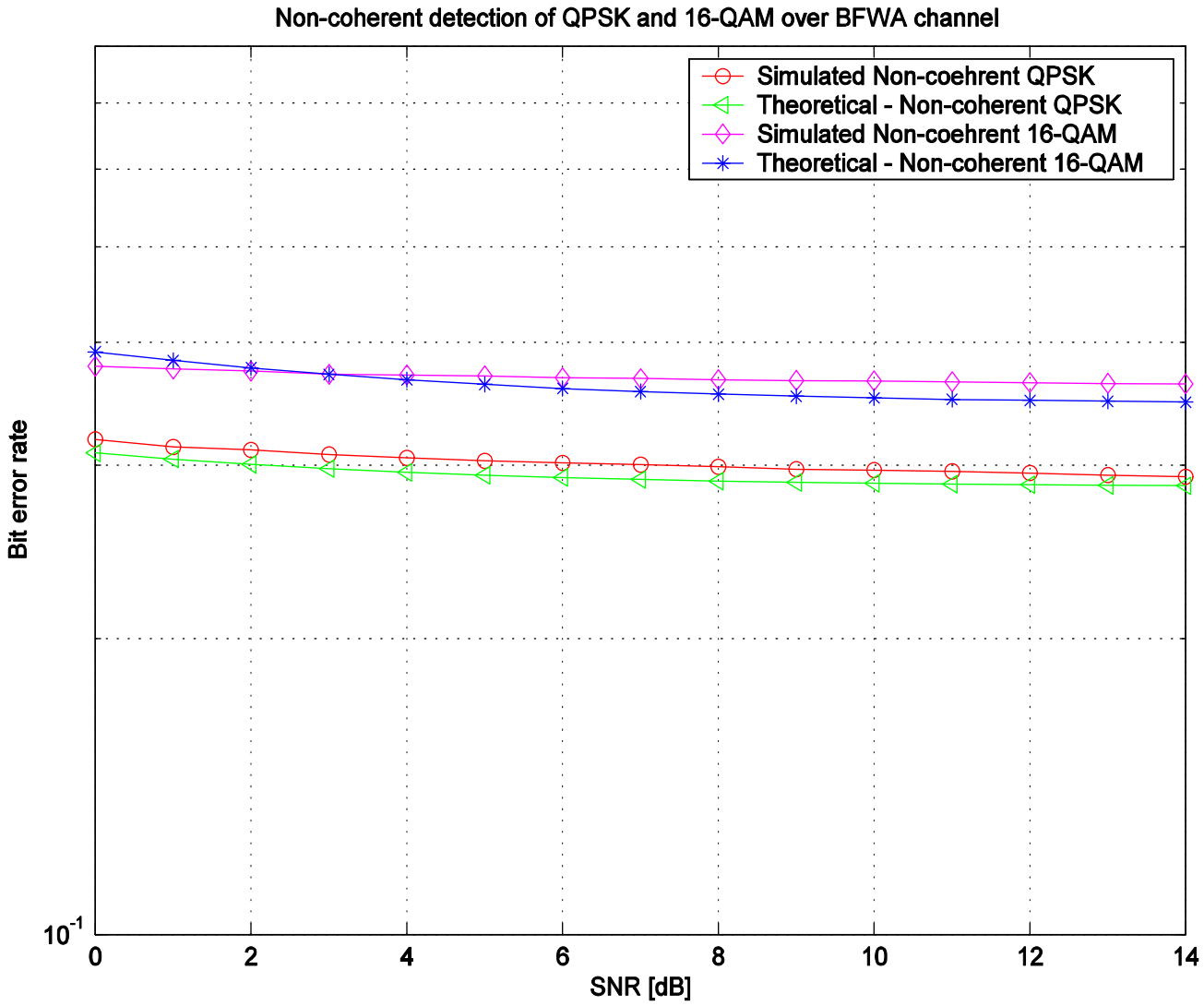
Non-coherent detection of QPSK and 16-QAM over BFWA channel
Simulated Non-coehrent QPSK
Theoretical - Non-coherent QPSK
Simulated Non-coehrent 16-QAM
Theoretical - Non-coherent 16-QAM
Bit error rate
10^-1
0
2
4
6
8
10
12
14
SNR [dB]

Figure 5

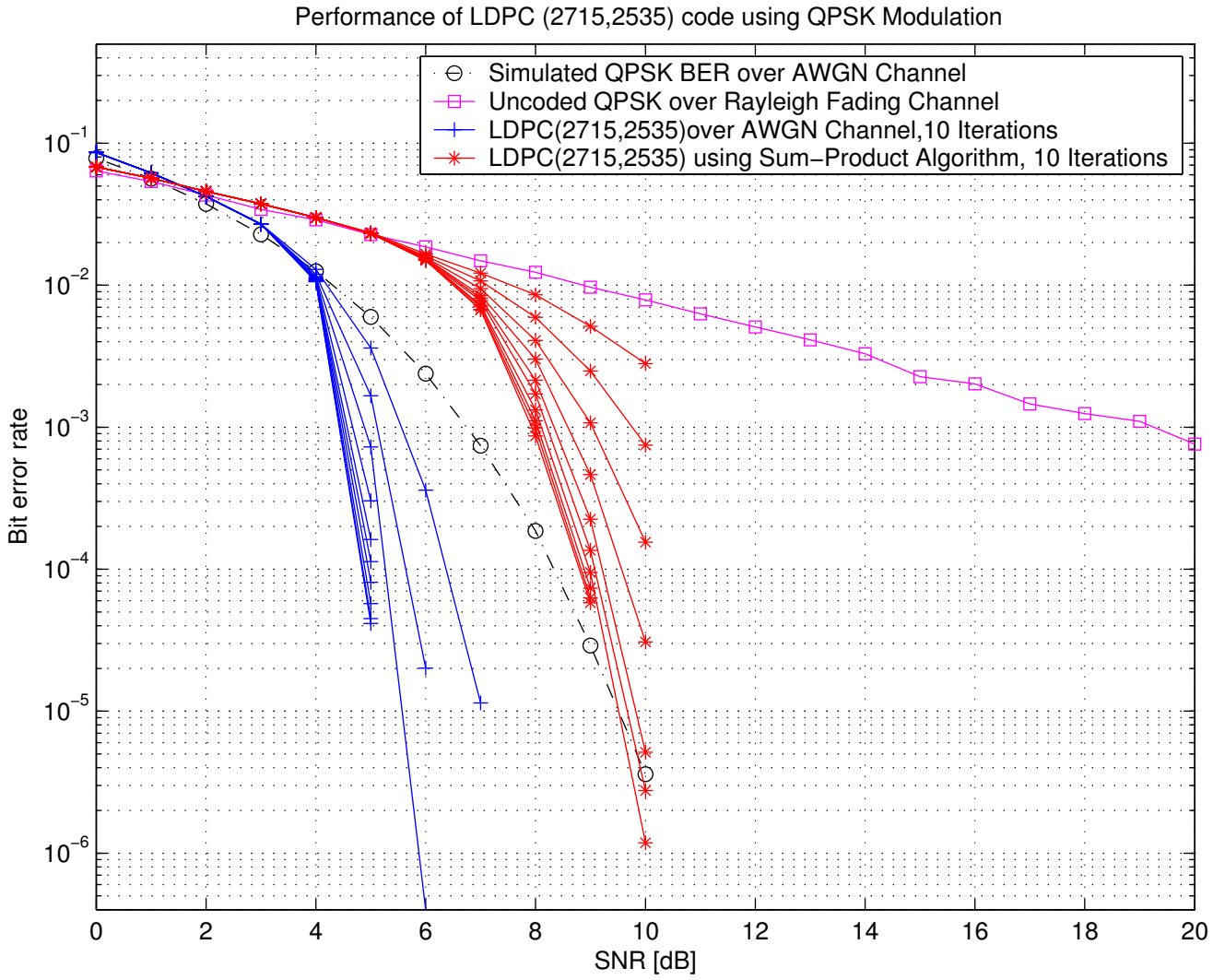
Performance of LDPC (2715,2535) code using QPSK Modulation
Simulated QPSK BER over AWGN Channel
Uncoded QPSK over Rayleigh Fading Channel
LDPC(2715,2535)over AWGN Channel,10 Iterations
LDPC(2715,2535) using Sum−Product Algorithm, 10 Iterations
Bit error rate
SNR [dB]
10^−1
10^−2
10^−3
10^−4
10^−5
10^−6
0
2
4
6
8
10
12
14
16
18
20

Figure 6

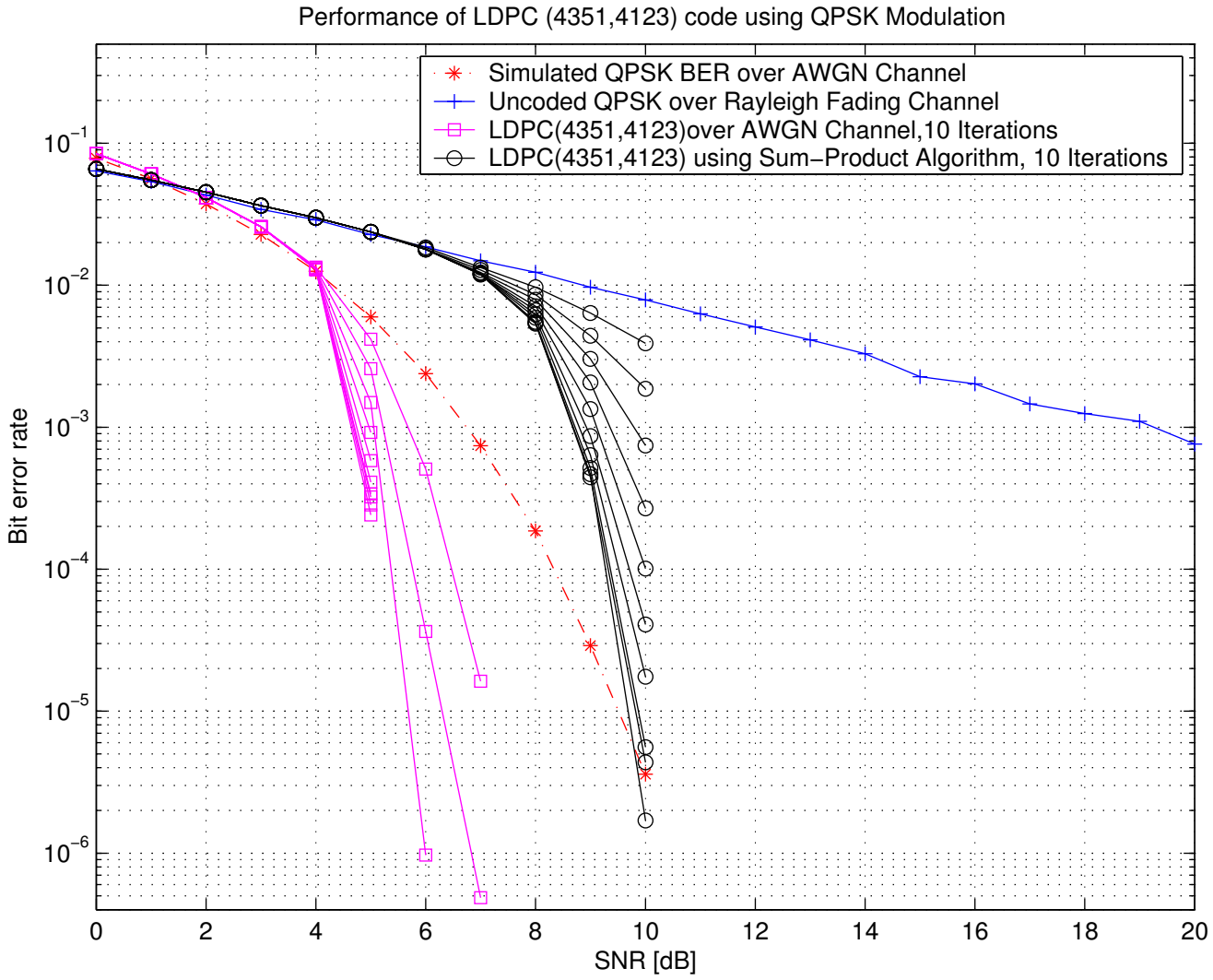
Performance of LDPC (4351,4123) code using QPSK Modulation
Simulated QPSK BER over AWGN Channel
Uncoded QPSK over Rayleigh Fading Channel
LDPC(4351,4123)over AWGN Channel,10 Iterations
LDPC(4351,4123) using Sum−Product Algorithm, 10 Iterations
Bit error rate
SNR [dB]
10^−1
10^−2
10^−3
10^−4
10^−5
10^−6
0
2
4
6
8
10
12
14
16
18
20

Figure 7

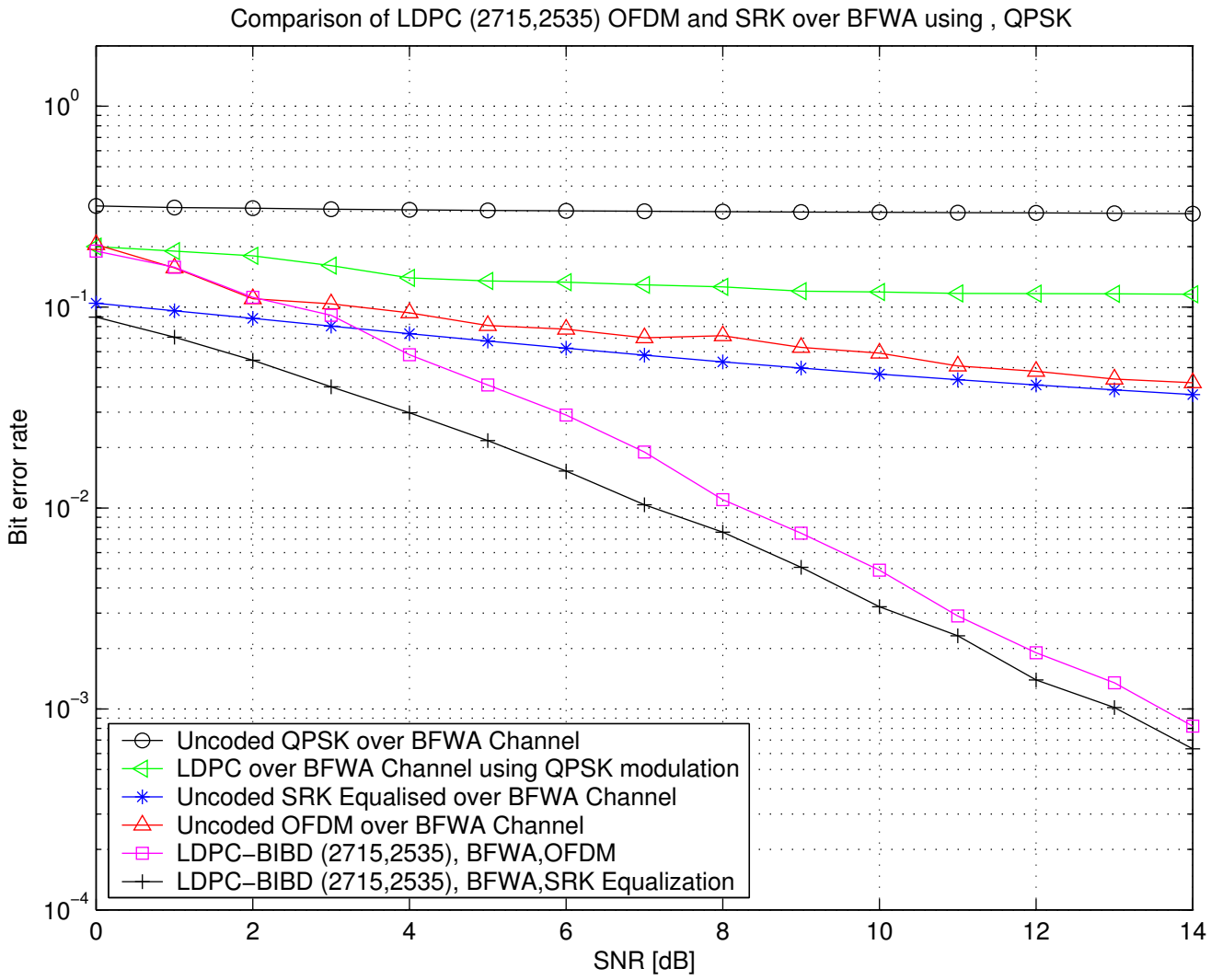
Comparison of LDPC (2715,2535) OFDM and SRK over BFWA using , QPSK
Bit error rate
SNR [dB]
Uncoded QPSK over BFWA Channel
LDPC over BFWA Channel using QPSK modulation
Uncoded SRK Equalised over BFWA Channel
Uncoded OFDM over BFWA Channel
LDPC−BIBD (2715,2535), BFWA,OFDM
LDPC−BIBD (2715,2535), BFWA,SRK Equalization

Figure 8

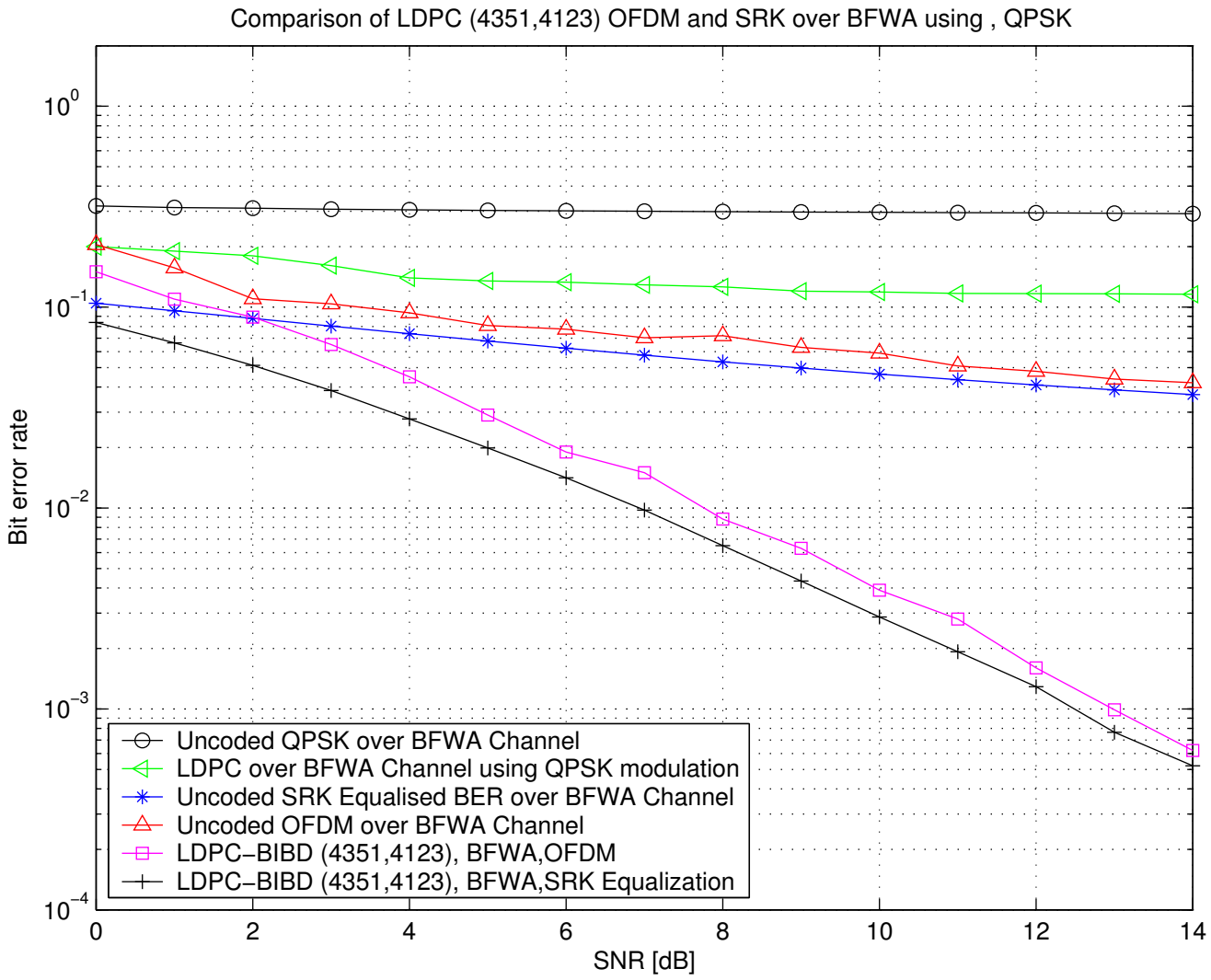
Comparison of LDPC (4351,4123) OFDM and SRK over BFWA using , QPSK
Bit error rate
SNR [dB]
Uncoded QPSK over BFWA Channel
LDPC over BFWA Channel using QPSK modulation
Uncoded SRK Equalised BER over BFWA Channel
Uncoded OFDM over BFWA Channel
LDPC−BIBD (4351,4123), BFWA,OFDM
LDPC−BIBD (4351,4123), BFWA,SRK Equalization

Figure 9

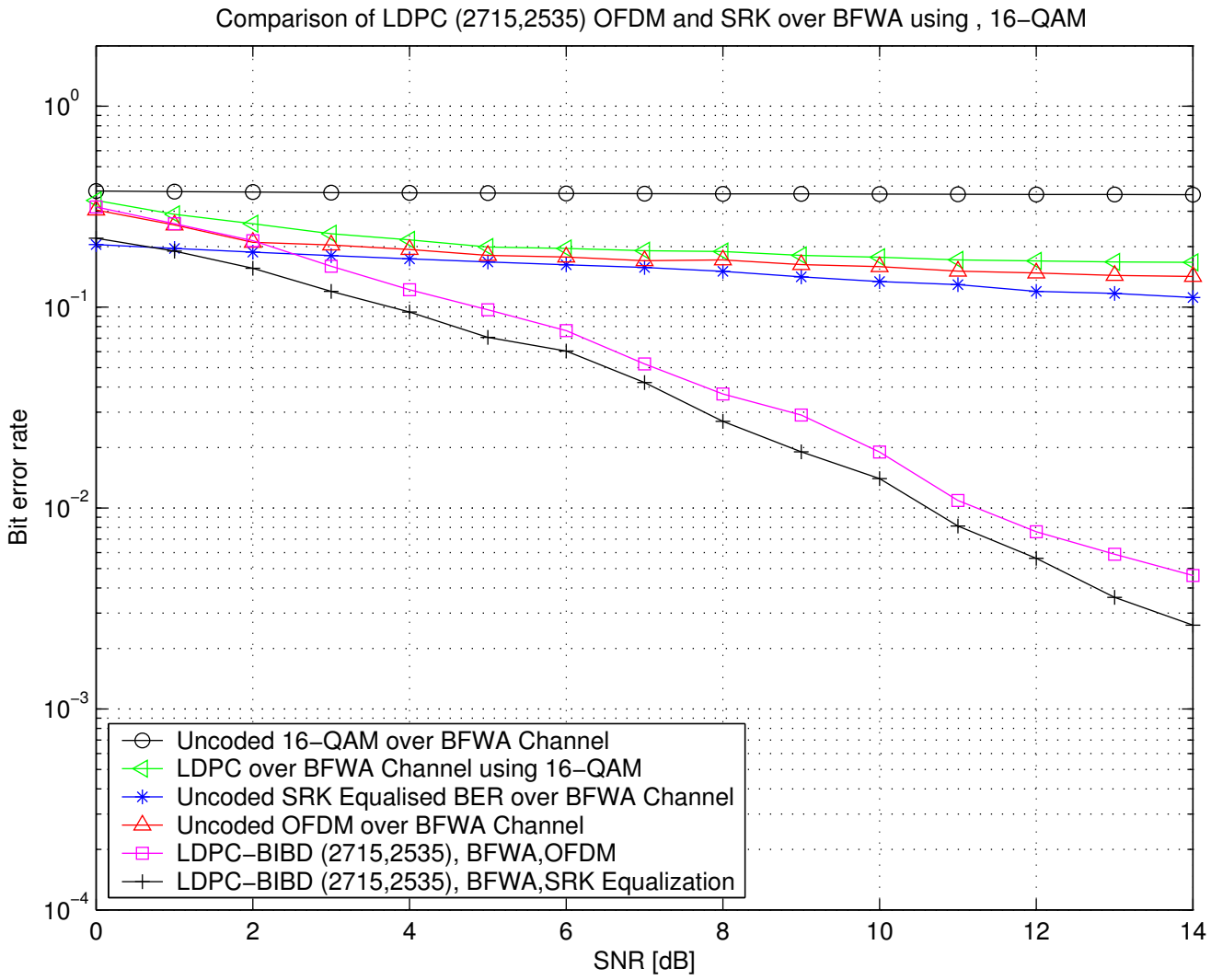
Comparison of LDPC (2715,2535) OFDM and SRK over BFWA using , 16−QAM
Bit error rate
SNR [dB]
Uncoded 16−QAM over BFWA Channel
LDPC over BFWA Channel using 16−QAM
Uncoded SRK Equalised BER over BFWA Channel
Uncoded OFDM over BFWA Channel
LDPC−BIBD (2715,2535), BFWA,OFDM
LDPC−BIBD (2715,2535), BFWA,SRK Equalization

Figure 10

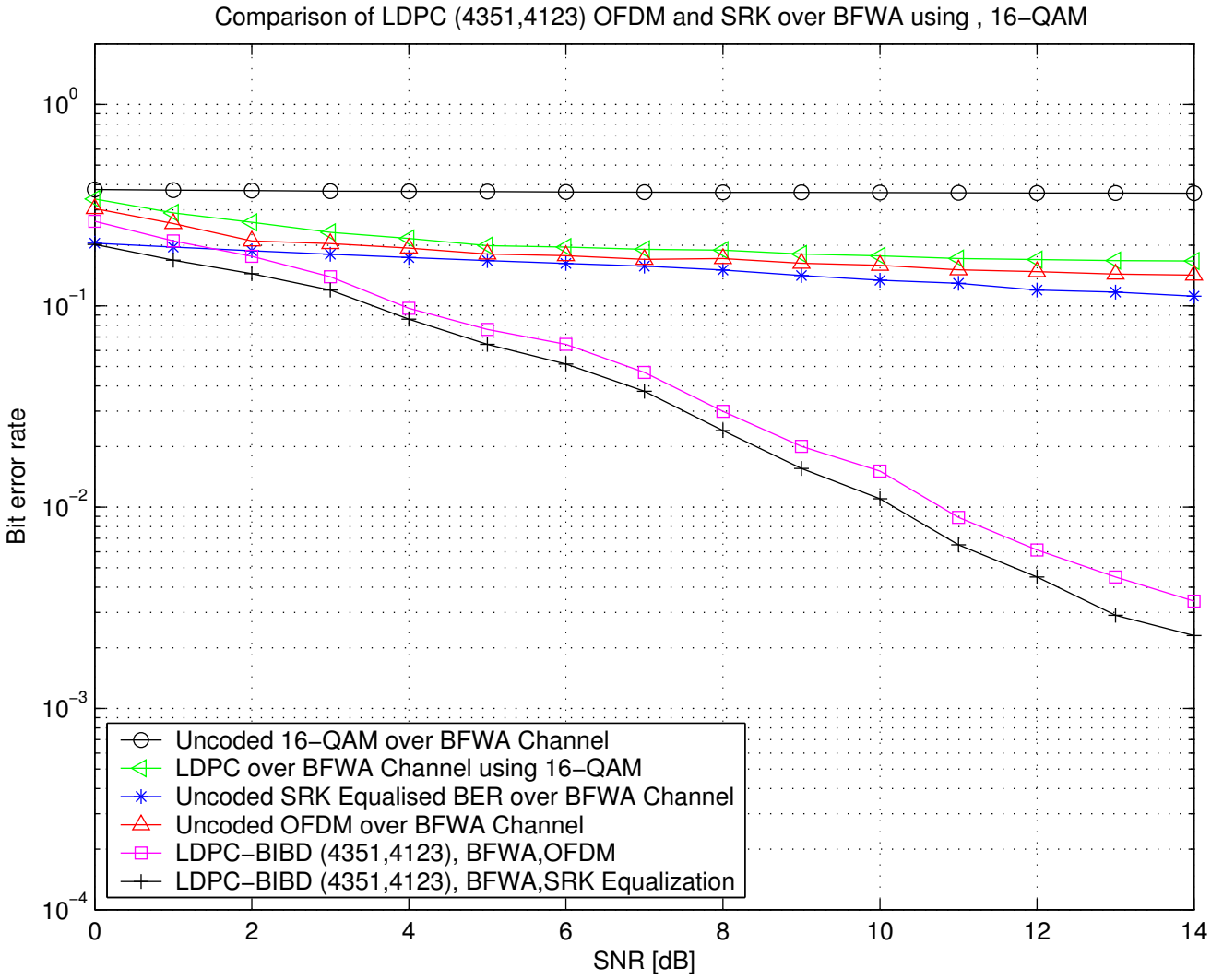
Comparison of LDPC (4351,4123) OFDM and SRK over BFWA using , 16−QAM
Bit error rate
SNR [dB]
Uncoded 16−QAM over BFWA Channel
LDPC over BFWA Channel using 16−QAM
Uncoded SRK Equalised BER over BFWA Channel
Uncoded OFDM over BFWA Channel
LDPC−BIBD (4351,4123), BFWA,OFDM
LDPC−BIBD (4351,4123), BFWA,SRK Equalization